PHYSICAL REVIEW B **84**, 134425 (2011)

All-optical subnanosecond coherent spin switching in thin ferromagnetic layers

Ettore Carpene*
CNR-IFN, Dipartimento di Fisica, Politecnico di Milano, Piazza Leonardo da Vinci 32, I-20133 Milano, Italy

Christian Piovera and Claudia Dallera
Dipartimento di Fisica, Politecnico di Milano, Piazza Leonardo da Vinci 32, I-20133 Milano, Italy

Eduardo Mancini
Institut für Experimentelle und Angewandte Physik, Universität Regensburg, Universitätsstrasse 31, D-93040 Regensburg, Germany

Ezio Puppin
CNISM, Dipartimento di Fisica, Politecnico di Milano, Piazza Leonardo da Vinci 32, I-20133 Milano, Italy
(Received 7 September 2011; revised manuscript received 29 September 2011; published 18 October 2011)

The need for faster magnetic recording devices has driven researchers to seek more efficient ways to reverse the magnetization. A large variety of methods and materials has been investigated to accomplish the most rapid spin reorientation, ranging from magnetic field pulses in ferromagnetic compounds to ultrashort optical excitations in ferrimagnetic and antiferromagnetic materials. To date, the precessional motion in an external field is the most effective route to control the magnetization in ferromagnets. Reversible switching under simple experimental conditions, i.e., in air and at room temperature, with a moderate optical excitation is a goal that has not been reached so far. Here we demonstrate that, using short laser pulses, the magnetization of a thin biaxial ferromagnetic layer can be optically and repeatedly commuted between well-defined directions on a time scale of 100 ps.

DOI: 10.1103/PhysRevB.84.134425 PACS number(s): 78.47.−p, 78.20.Ls, 75.70.−i

I. INTRODUCTION

Ferromagnetic materials normally used in magnetic storage devices possess a preferential direction called "easy axis" along which the magnetization can be either parallel ("up" state) or antiparallel ("down" state). Recording a bit of information means switching the magnetization along this axis, and one of the most challenging technological issues is to achieve the fastest writing speed. The ultrafast magnetization reversal can be promoted by rapid magnetic field pulses or by ultrashort optical excitations. The optical route is being explored for materials showing all different kinds of magnetic order, i.e. ferromagnets,[1] ferrimagnets[2] and antiferromagnets.[3,4] Experiments on metallic ferromagnets have shown precessional magnetization reversal induced by strong magnetic fields[5,6] or intense optical pulses[1] on the few hundreds of picoseconds time scale, although the existence of an ultimate switching speed due to the emergence of stochastic processes has been demonstrated.[7] A class of compounds that is receiving increasing attention is the ferrimagnetically ordered one, where the presence of two magnetic subarrays allows us to achieve reversal of the magnetization by going through a nonequilibrium state. In GdFeCo [Refs. 8, 9] the process takes place within 30 ps close to the compensation temperature, when the domain wall mobility is the largest. More recently, antiferromagnets are attracting the attention of the scientific community since the discovery of inertia-driven subpicosecond spin reorientation.[3,4]

An intriguing possibility, so far scouted only in (Ga,Mn)As magnetic semiconductors,[10,11] is offered by materials with biaxial magnetic anisotropy, resulting in the presence of two equivalent preferential axes (i.e., four likely orientations of the magnetization), thus allowing one to record two bits of information on the same spot. Recent experiments on (Ga,Mn)As have shown a large photoinduced reduction of the coercive field that leads to magnetization reversal.[12] The recovery time of the coercivity was found to be in the few nanoseconds range, which sets the maximum writing speed for this material. A practical drawback of (Ga,Mn)As is its Curie temperature of 25 K, which requires cooling facilities during the experiment.

In our experiment we have realized a straightforward method for controlling the magnetization of the simplest ferromagnet, i.e., iron, by exploiting its biaxial magnetic anisotropy and using only optical pulses. The samples investigated here are thin Fe(001) films (about 8 nm thick) epitaxially grown on MgO(001) single crystals. For this thickness, the magnetization **M** lies on the film plane, and the epitaxial nature of the metallic layer leads to preferential in-plane orientations of the magnetic vector along the [100] or [010] crystallographic directions (the easy axes), a direct consequence of the magnetocrystalline anisotropy.[13]

By applying a magnetic field **H** along the film surface but not aligned to an easy axis [see Fig. 1(a)], the magnetization vector will coherently rotate assuming the in-plane orientation that minimizes the free energy $G = K_1 \sin(2\phi)^2/4 - \mathbf{M}\cdot\mathbf{H}$ (here K_1 is the magnetocrystalline anisotropy constant and ϕ is the angle between **M** and the [100] direction).[14] A peculiar situation is achieved when the external field points *between* easy axes [i.e., at an angle $\theta \simeq 44^\circ$ (Ref. 15)]: in such a case, as shown in Fig. 1(b), there are two almost-symmetric minima of the free energy close to the [100] and to the

 ©2011 American Physical Society

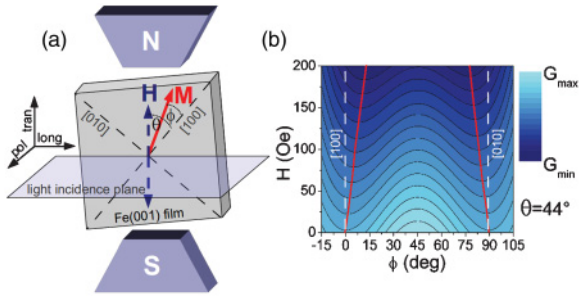

FIG. 1. (Color online) (a) The epitaxial Fe(001) film has two in-plane easy axes along the [100] and [010] crystallographic directions. The external magnetic field is applied in the transverse direction, along the film and normal to the light incidence plane. The longitudinal direction is parallel to the film and the incidence planes, and the polar direction is normal to the film. θ and ϕ are the angles formed by the field and the magnetization, respectively, with the [100] axis. (b) Free-energy contour plot (in false colors) as a function of ϕ (horizontal) and H (vertical) depicting the energy minima (red solid lines) that correspond to the equilibrium orientation of the magnetization. The graph refers to an angle $\theta = 44^\circ$ between the applied field and the [100] axis.

[010] crystallographic directions, even for relatively weak external fields (a few hundreds of Oe). We will show here that it is possible to systematically and repeatedly switch the magnetization between these two minima using short laser pulses, with a switching time of the order of 100 ps.

II. EXPERIMENTAL RESULTS

The measurements are based on the time-resolved magneto-optical Kerr effect (TRMOKE), a technique that allows one to retrieve the magnetization state of a ferromagnetic sample by detecting the polarization rotation of light reflected from its surface as a function of time.[16] It relies on the pump-probe method by means of femtosecond laser pulses, and it has been successfully employed in the last 15 years to investigate several aspects of magnetic phenomena thanks to its subpicosecond time resolution[17–22] and its capability to detect the real-space components of the magnetization vector.[23–26] The experiments are performed at room temperature with a Ti:sapphire laser system operating at 800 nm with a pulse duration of 50 fs and a repetition rate of 1 kHz. The TRMOKE signal is detected while slowly varying an external magnetic field applied along the Fe layer and normal to the light incidence plane [the so-called transverse direction; see Fig. 1(a)]. Thus, each probing pulse records the signal at a different field intensity, allowing us to retrieve thorough information on the magnetic state of the sample. In order to investigate the effect of multiple pump pulses on the magnetization, the repetition rate of the probe beam is reduced to 250 Hz, and a proper temporal sequence of pump, probe, and an additional pulsed magnetic field, used to restore the unirradiated condition after each probe, is employed (details can be found in Appendix A).

Figure 2 reports the hysteresis loops in the transverse direction, i.e., parallel to the external field [Fig. 2(a)], and in the longitudinal direction, i.e., in plane and normal to the external field [Figs. 2(b)–2(e)]. Each point of the loop is measured after irradiating the sample with a given number

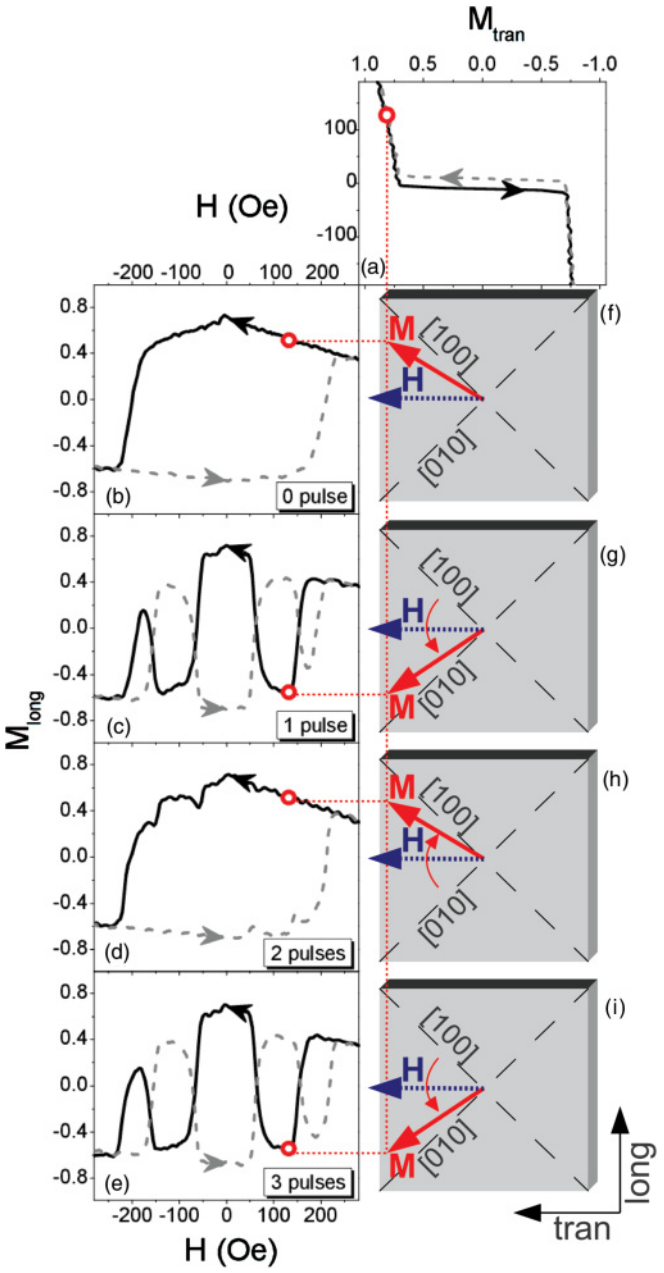

FIG. 2. (Color online) (a) Transverse and (b)–(e) longitudinal hysteresis loops showing the modification induced on the magnetization by increasing the number of laser pump pulses: zero pulses (a, b), one pulse (c), two pulses (d), and three pulses (e). The external magnetic field H is applied along the transverse direction [refer to Fig. 1(a)] at an angle $\theta \simeq 44^\circ$ from the [100] crystallographic axis. The red circles in (a)–(e) mark the magnetization components at the external field $H = +130$ Oe on the same branch of the loops: they are used to visualize the real-space orientation of **M** on the sample plane at $H = +130$ Oe, as sketched in (f)–(i). These cartoons clearly demonstrate how the magnetic vector systematically and repeatedly commutes between two easy axes after each optical excitation.

of laser pump pulses, ranging from zero [Fig. 2(b)] to three [Fig. 2(e)]. The transverse hysteresis loop is reported only once since it does not vary with the number of pump pulses. In the following discussion, we will focus on the branch of the hysteresis loops obtained spanning the external field from

positive to negative values (solid lines). The other branch (dashed lines) leads to identical results. The small colored circles in Figs. 2(a)–2(e) mark the projections M_{tran} and M_{long} for a specific intensity of the external field $H = +130$ Oe. They are used to visualize the real-space orientation of the magnetization vector at this particular value of H and after the corresponding number of pump pulses, as sketched in Figs. 2(f)–2(i). In this experiment, the time delay between pump and probe is at least 1 ms, long enough to ensure the absence of transient effects. The ultrafast evolution of the magnetization will be analyzed in the second part of this paper. The "zero-pulse" case [Figs. 2(a), 2(b), and 2(f)] denotes the absence of optical excitations: the magnetization vs the external field shows sharp transitions in correspondence to the coercive fields of about 10 Oe in the transverse direction [Fig. 2(a)] and 200 Oe in the longitudinal direction [Fig. 2(b)]. These transitions correspond to the magnetization jumping from one easy axis to the other through domain wall motion.[14,27] It should be noticed that for an external field of +130 Oe [Fig. 2(f)], the magnetization vector points close to the [100] easy axis. After one optical excitation ["one-pulse" case, Figs. 2(c) and 2(g)], the transverse loop (not reported here) is unaffected, but the longitudinal projection clearly reveals that, within a well-defined range of external field values around ±130 Oe, M_{long} has reversed its sign [Fig. 2(c)]. Correspondingly, at $H = +130$ Oe the magnetization vector has switched from the [100] easy axis to the [010] one [Fig. 2(g)]. For higher or lower intensities of the external field, no change is observed as compared to the "zero-pump" case. After two pump shots ["two-pulse" case, Figs. 2(d) and 2(b)], the longitudinal hysteresis loop [Fig. 2(d)] has recovered the original shape of the nonirradiated sample [Fig. 2(b)]. In particular, for applied field of +130 Oe, the magnetization vector has switched back to the initial orientation, close to the [100] axis [Fig. 2(h)], assumed before any optical excitation [Fig. 2(f)]. Finally, the third laser shot ["three-pulse" case, Figs. 2(e) and 2(i)] reproduces the features observed after the first pulse [Figs. 2(c) and 2(g)]. Although not shown here, we have tested the perfect reproducibility of these events up to nine laser pump shots. These measurements demonstrate that the magnetization vector can be repeatedly and reproducibly switched between two given orientations with short optical pulses. However, the commutation between easy axes takes place only for specific intensities of the external field, in particular, for $H \sim 130$ Oe. Higher or lower magnetic fields do not lead to any switching.

In order to clarify the physical mechanism and disclose the time scale of the process, we have analyzed the temporal evolution of the magnetization triggered by a single pump pulse for two fixed values of H: +130 and +230 Oe, where only the lower field results in a switched magnetic vector. Figure 3 reports the polar (normal to the sample) and longitudinal components of the magnetization vector as a function of the pump-probe delay for the two aforementioned intensities of the external magnetic field. We begin analyzing the results for $H = +130$ Oe [Figs. 3(a)–3(c)]. At zero pump-probe delay, the polar component [Fig. 3(a)] is absent (within the experimental errors), while the longitudinal projection [Fig. 3(b)] has positive value. Recalling Figs. 2(b) and 2(f), this situation corresponds to the magnetization vector being on the film plane and pointing close to the [100] crystallographic axis. As the time delay increases, the polar projection shows a damped oscillatory behavior, while the longitudinal projection changes sign within 100 ps and oscillates around a new equilibrium position centered at negative values. Although the dynamics is restricted to a time interval of 500 ps, the oscillations will eventually stop, and the magnetization will settle close to the [010] crystallographic direction, as observed in Fig. 2(c), which depicts the situation after a pump-probe delay of 1 ms. Figure 3(c) reports the reconstruction of the magnetization trajectory projected on the plane perpendicular to the external field. Here the route of the magnetic vector and the precessional nature of the process are particularly evident. If we now consider the magnetization dynamics for $H = +230$ Oe [Figs. 3(d)–3(f)], the situation at zero delay is

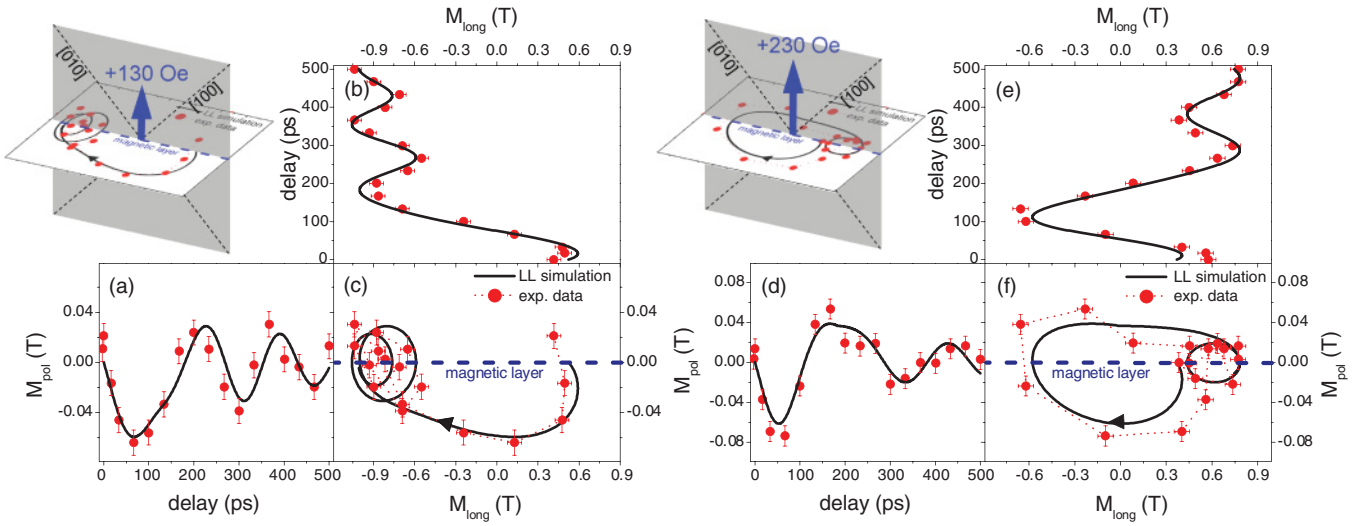

FIG. 3. (Color online) Evolution of the magnetization as a function of the pump-probe delay for two intensities of the external field: (a)–(c) +130 Oe and (d)–(f) +230 Oe. The red dots are the experimental data, and the solid lines are the simulation according to the LL equation [Eq. (1)]. The polar (a),(d) and the longitudinal (b),(e) components are used to reconstruct the magnetization trajectory (c, f) projected on the plane normal to the external field [as schematically sketched on top of (a) and (d)].

similar to the one previously described, with the magnetization lying on the film plane and pointing close to the [100] axis. After 100 ps, the longitudinal component [Fig. 3(e)] has fully reversed its sign, but at 250-ps delay it has recovered its original orientation. From this point on, no further switching is observed, and only the damped oscillatory behavior is noticeable. As in the previous case, the magnetization trajectory projected on the plane perpendicular to the external field [Fig. 3(f)] markedly reveals the precessional behavior.

The phenomenological description of the magnetization dynamics in a magnetic field is described by the Landau and Lifshitz (LL) equation:[28]

$$\frac{\partial \mathbf{M}}{\partial t} = -\gamma \mathbf{M} \times \mathbf{H}_{\text{eff}} - \gamma \frac{\alpha}{M} \mathbf{M} \times (\mathbf{M} \times \mathbf{H}_{\text{eff}}), \qquad (1)$$

where γ is the gyromagnetic ratio and α is a damping coefficient. $\mathbf{H}_{\text{eff}} = \mathbf{H} + \mathbf{H}_{an} + \mathbf{H}_{\text{dem}}$ is the effective magnetic field acting on $\mathbf{M}$: it is the sum of the external field $\mathbf{H}$, the anisotropy $\mathbf{H}_{an}$, and the demagnetizing field $\mathbf{H}_{\text{dem}}$. In our specific case of a thin epitaxial Fe layer with the magnetization lying on the film plane, the demagnetizing field acts only on the out-of-plane component of $\mathbf{M}$, while the combined effect of external and magnetic anisotropy fields can be deduced from the angular dependence of the free energy.[27] A nontrivial complication, however, is the fact that the magnetization dynamics is triggered by an intense optical pulse acting as a heat source, thus resulting in a time-dependent temperature of the irradiated area. Since $\mathbf{M}$, $\mathbf{H}_{an}$, and $\mathbf{H}_{\text{dem}}$ are all temperature-dependent quantities, they indirectly acquire specific time dependencies that cannot be neglected. Taking all these aspects into account, the LL equation has been numerically solved: the simulations of the magnetization trajectories for the two values of the external field (+130 and +230 Oe) are reported in Fig. 3 as solid lines, showing a satisfactory agreement with the experimental data (details can be found in Appendix B).

III. DISCUSSION

At this point the results need further discussion. Using tens of femtoseconds laser pulses as excitation, the different degrees of freedom in the solid (electrons, spins, and lattice) react on different time scales. It is well established that the local thermal equilibrium settles within a few picoseconds.[16,22] Thus, on a time scale of several tens of picoseconds, the laser pumping can be viewed as a local heat source, rapidly increasing the temperature of the irradiated volume. Subsequently, the excited zone of the sample cools with a characteristic rate that is essentially determined by the heat transport properties of the material (and of the substrate). The temporal evolution of the temperature governs also the time dependencies of the magnetization and anisotropy field. In order to obtain them, we first examined the time-dependent modulus of the normalized magnetization $M_{\text{norm}}(t)$ experimentally measured at remanence (where no precession is present), as reported in Fig. 4(a) (red dots). Since the temperature dependence $M(T)$ of the magnetization in iron is known,[30] a temporal profile $T(t)$ of the local temperature can be numerically extracted from the magnetization data. Furthermore, the temperature dependence of the crystalline anisotropy in iron is known.[29] Thus, using the estimated $T(t)$, the temporal evolution of the anisotropy field $H_{an}(t)$ is obtained. The solid curves shown in Fig. 4 are the

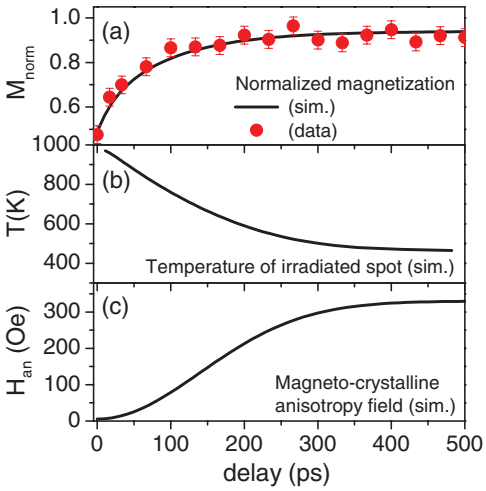

FIG. 4. (Color online) Temporal evolution of (a) the normalized modulus of the magnetization, (b) the local temperature in the irradiated spot, and (c) the intensity of the magnetocrystalline anisotropy field. Solid lines are the simulation used to numerically solve the LL equation. The normalized magnetization in (a) is compared with the experimental data (red dots) measured at remanence (i.e., with no external field), where no precessional motion is present.

results of this procedure, and they represent the optimized time dependencies of the magnetization [Fig. 4(a)], local temperature [Fig. 4(b)], and the anisotropy field [Fig. 4(c)] used in the LL equation.

According to our analysis, the maximum local temperature in the irradiated spot is about 1000 K [see Fig. 4(b)], thus very close to the Curie point of iron (1043 K). Correspondingly, the anisotropy field [which is about 500 Oe at 300 K (Ref. 13) and has a strong temperature dependence[29]] drastically drops to zero and then slowly recovers as the temperature of the irradiated spot decreases [see Fig. 4(c)]. Within the first 100 ps, H_{an} is much weaker than the external fields considered in our previous analysis (130 and 230 Oe). Thus, the effective field $\mathbf{H}_{\text{eff}}$ is mainly determined by $\mathbf{H}$ (plus the demagnetizing field acting on the out-of-plane component of $\mathbf{M}$). Consequently, during this time interval the precession of the magnetic vector occurs around $\mathbf{H}$. Since the latter points in the transverse direction, i.e., at the highest angular distance from $\mathbf{M}$, the amplitude of the gyroscopic motion is large enough to determine the longitudinal switching observed in Figs. 3(b) and 3(e). At longer delays (>150 ps), the anisotropy field, which has its maximum intensity along the easy axes, recovers and overcomes the values of the external field. Therefore, the effective field is mainly determined by $\mathbf{H}_{an}$, and the precessional motion occurs around an easy axis. Keeping in mind that the frequency of the precession increases with the field intensity,[27,31] within the first 100 ps past the optical excitation and for $H =$ 230 Oe, the magnetization vector performs an almost complete orbit around $\mathbf{H}$ before the intensity of the anisotropy field is large enough to *trap* the magnetization around an easy axis [see Fig. 3(f)]. For $H = 130$ Oe, on the other hand, the precession frequency is slower, and when the longitudinal projection of the magnetic vector has switched to negative values, the anisotropy field has already overcome H. In this case, the magnetization is trapped by $\mathbf{H}_{an}$ in the proximity of

the [010] easy axis [see Fig. 3(c)] and will eventually settle there, resulting in a switched magnetic orientation.

IV. CONCLUSIONS

To summarize, we have demonstrated that the magnetization in a thin epitaxial ferromagnetic layer with biaxial anisotropy can be controlled using short optical pulses. In particular, it is possible to reproducibly and repeatedly commute the magnetic vector between preferential directions with a proper orientation and intensity of the external field. The switching mechanism is thermally driven and relies on the magnitude of the external magnetic field relative to the time-dependent magnetic anisotropy field. The switching time is essentially determined by the applied field and resides in the 100-ps time window for our specific design. We believe these results can trigger the research of new materials with optimized parameters in view of a faster switching process, but they can also open interesting prospects on the continuously developing field of ultrafast magnetic recording.

ACKNOWLEDGMENTS

We wish to thank Gianluca Galzerano for his help in designing the experimental setup. The "Fondazione Cariplo" in gratefully acknowledged for the financial support.

APPENDIX A: THE EXPERIMENTAL SETUP

The thin Fe(001) films (about 8 nm thick) are epitaxially grown on MgO(001) single crystalline substrates of 1-cm lateral size. Prior to the deposition, the substrates have been cleaned by repeated cycles of sputtering with 1-kV Ar^+ ions and annealing at 800 K in ultrahigh vacuum. The Fe deposition is performed with an electron-beam evaporator at a rate of about 2 Å/min on the substrates at room temperature. After deposition, the samples are annealed at 750 K in order to reduce defects formed during the epitaxial growth and characterized by low-energy electron diffraction (LEED). The samples are allowed to oxidize in air, leading to the formation of a self-passivating, protecting FeO layer that extends for 2–3 nm at the most, removing 1–1.5 nm of Fe.[32,33]

The optical analysis is performed *ex situ* with an amplified Ti:sapphire laser, generating 50-fs pulses centered at 800 nm (1.55 eV) and a repetition rate of 1 kHz. The time resolution is achieved via the pump-probe technique. The *p*-polarized pump beam, with an average fluence of 12 mJ/cm^2, is focused on a spot size of about 140 μm, hitting the sample at an incident angle of $\sim 68^\circ$ with respect to the surface normal. The linearly polarized probe beam has a dimension of about 13 μm on the sample and an incidence angle of $\sim 42^\circ$. After reflection, the probe passes through an analyzer (Glan-Thomson polarizer) oriented at an angle $\theta_a = 45^\circ$ from the plane of incidence and is then detected by a photodiode. We employed the double-detector scheme in order to increase the sensitivity to the small MOKE signal.[22] The procedure to separate the three-dimensional (3D) components of the magnetization vector is based on the Fresnel scattering matrix formalism,[34] and a detailed description can be found elsewhere.[27] The external magnetic field **H** is produced by two Helmholtz coils and is applied normal to the incidence plane (thus parallel to the sample surface). The sample is oriented in order to form an angle $\theta \simeq 44^\circ$ between **H** and the [100] crystallographic direction. With this choice, the coercive field along the longitudinal direction is about 200 Oe (see Fig. 2), large enough to allow the observation of the magnetic commutation at $H = 130$ Oe, but small enough to allow recording the entire hysteresis loop with a moderate external field (a few hundred Oe at the most).

The hysteresis loops are measured sweeping continuously the external field between two opposite values (roughly ± 300 Oe) with a constant rate of about 1 kOe/s. In order to investigate the effect of multiple pump pulses on the magnetization, the repetition rate of the probe beam is reduced to 250 Hz. Between subsequent probes, an additional pulsed magnetic field is applied parallel to the external one [see Fig. 5(a)]. These field pulses, produced by short current bursts (about 0.4 ms long) through small coils, are synchronized with the probe ones (thus, at a repetition rate of 250 Hz) and are properly delayed in order to fall between two pump pulses. With the given sweeping rate of the external field ($\sim$1 kOe/s) and the repetition rate of the probe (250 Hz), the magnetization is sampled at field intervals of about 4 Oe. The scope of the pulsed magnetic field is to cancel the effect induced by all preceding pumps by rapidly bringing the magnetization to saturation and back. With a proper temporal sequence of the pump, probe, and magnetic field pulses, the modification induced by zero, one, two, and three pump irradiations can be investigated. The procedure is sketched in Fig. 5(b). Notice

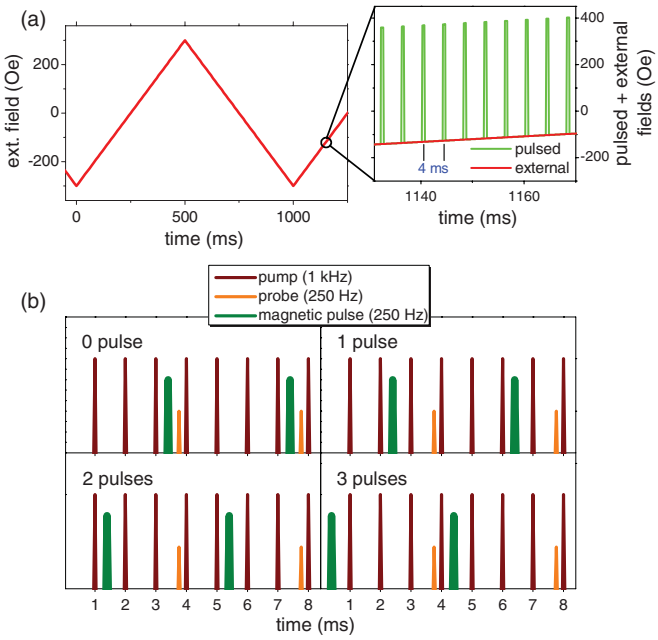

FIG. 5. (Color online) (a) The external magnetic field H sweeps continuously between two opposite values (± 300 Oe), with a rate of about 1 kOe/s. Additionally (see inset), short (0.4 ms) and intense (about 0.5 kOe) magnetic field pulses are applied parallel to **H** at the frequency of the probe, i.e., 250 Hz. The magnetic pulses can be either positive (as in the inset) or negative. (b) The temporal sequence of pump, probe, and magnetic field pulses can be modified in order to study the effects of zero, one, two, and three pump irradiations on the magnetization (see text).

that the probe shortly precedes the nearest pump pulse by a fixed delay (a few picoseconds). When the pulsed magnetic field falls right before the probe (zero-pulse case), the effects of all previous pumps are canceled. In this case, the hysteresis loop can be measured with the sweeping external field as if no optical excitation was present. When one pump falls between the probe and the pulsed magnetic field (one-pulse case), each probe will detect the modification induced by a single pumping. With the sweeping field running, it is possible to study the effect of a single pump as a function of the intensity of the external field. Similarly, when two or three laser pumps fall between the magnetic pulse and the probe (two-pulse and three-pulse cases, respectively), each probe samples the changes produced by two or three subsequent laser irradiations on the magnetic state of the film. It should be mentioned that, in the presence of the pulsed magnetic field, only one branch of the hysteresis loop can be measured. An example will clarify this point. Let's assume that the sweeping external field is starting from negative intensity (about −250 Oe) and the pulsed magnetic field is positive but intense enough (about +500 Oe) to saturate the magnetization in the opposite direction. Each magnetic pulse will rapidly guide the magnetic vector to saturation through one branch (the up branch) of the hysteresis loop. When the pulsed field ends (within 0.4 ms), only the negative external field is present, and the magnetization will return to its initial magnitude and orientation through the other branch (the down branch) of the loop. As the intensity of the external field increases, the process will repeat in the same way. Therefore, with positive pulsed field we can only measure the branch of the hysteresis loop that would be obtained without pulses and sweeping the external field from positive to negative intensity (down branch). To measure the opposite branch of the loop, the pulsed field has to be inverted. By reducing the probe frequency (and correspondingly the pulsed magnetic field frequency) to 100 Hz, we have verified that the optically induced commutation of the magnetization vector (as previously described; see Fig. 2) is perfectly reproducible up to nine laser pump shots.

The dynamics of the magnetization vector (Fig. 3) is measured starting from the zero-pulse case and delaying the probe with respect to the pump in the temporal window of 0–500 ps. The procedure to extract polar and longitudinal components of the magnetization from the MOKE signal is reported in Ref. 27.

APPENDIX B: NUMERICAL SOLUTION OF THE LL EQUATION

The phenomenological description of the magnetization dynamics in a magnetic field is described by the LL equation:[28]

$$\frac{\partial \mathbf{M}}{\partial t} = -\gamma \mathbf{M} \times \mathbf{H}_{\text{eff}} - \gamma \frac{\alpha}{M} \mathbf{M} \times (\mathbf{M} \times \mathbf{H}_{\text{eff}}), \qquad \text{(B1)}$$

where $\gamma = e/m$ is the gyromagnetic ratio (e and m are the electron charge and mass, respectively) and α is a damping coefficient. We will conventionally label the components of the magnetization as $M_{\text{long}} = M_x$, $M_{\text{tran}} = M_y$, and $M_{\text{pol}} = M_z$. The effective magnetic field $\mathbf{H}_{\text{eff}}$ is the sum of the external field $\mathbf{H}$ (applied along the film), the crystalline anisotropy field $\mathbf{H}_{an}$, and demagnetizing field $\mathbf{H}_{\text{dem}}$. For thin magnetic layers, the *shape* anisotropy forces the magnetization to lie on the film plane, and the demagnetizing field (which equals in modulus the magnetization) manifests itself only on the out-of-plane component M_z. The combined effect of the external field and the crystalline anisotropy is an in-plane field $\mathbf{A}$ that can be deduced from the free energy of the magnetic system $G = K_1 \sin(2\phi)^2/4 - MH\cos(\phi - \theta)$.[14] K_1 is the anisotropy constant, and ϕ and θ are the angles formed by $\mathbf{M}$ and $\mathbf{H}$, respectively, with the [100] easy axis. Under static equilibrium conditions, $\mathbf{M}$ and $\mathbf{A}$ must be parallel: in fact, if $\mathbf{M}$ were misaligned with respect to $\mathbf{A}$, it would experience a torque, contradicting the equilibrium statement. Thus, ϕ is also the angle between $\mathbf{A}$ and the [100] axis. Under dynamical conditions, if the magnetization is subject to a precessional motion, it will eventually converge toward the orientation of $\mathbf{A}$. Recalling that, for a biaxial system like the Fe(001) film, the anisotropy field is $H_{an} = 2K_1/M$,[13] the free energy can be written as $g = G/M = H_{an}\sin(2\phi)^2/8 - H\cos(\phi - \theta)$, which has the dimension of a magnetic field. The modulus A and orientation ϕ of the in-plane field can be deduced by numerically solving the following equations:[27]

$$\partial g/\partial \phi = H_{an}\sin(4\phi)/4 + H\sin(\phi - \theta) = 0, \qquad \text{(B2)}$$

$$\partial^2 g/\partial \phi^2 = H_{an}\cos(4\phi) + H\cos(\phi - \theta) = A. \qquad \text{(B3)}$$

The latter, in particular, is exactly the expression of the in-plane field that can be obtained from the theory of ferromagnetic resonance.[31] It should be noticed that, due to the effect of the pump pulse, the local temperature of the irradiated spot varies in time. Therefore H_{an} (which strongly depends on the temperature) and, consequently, ϕ and A are all time-dependent quantities, i.e., $H_{an}(t)$, $A(t)$, and $\phi(t)$. The laser pulse affects also the modulus of the magnetization M, which acquires a specific time dependence $M(t)$. The latter can be experimentally measured (see Fig. 4) and used as a known parameter in the simulations. Moreover, since the temperature dependence of the magnetization is known,[30] we can numerically estimate the temperature profile $T(t)$ (this procedure is described in Ref. 26). Using the known temperature dependence of the anisotropy constant K_1 (Ref. 29) and the definition of H_{an}, we can deduce $H_{an}(t)$ and, from Eqs. (B2) and (B3), $A(t)$ and $\phi(t)$. Referring to Fig. 6(a) for the angular relations, $\mathbf{A}$ can be expressed in terms of Cartesian components to be used in the LL equation as $A_x = A\cos(\pi/2 - \theta + \phi)$, $A_y = A\sin(\pi/2 - \theta + \phi)$, $A_z = 0$.

Since the modulus of the magnetization vector is known from the experiment, its orientation can be expressed in terms of spherical coordinates as $M_x = M\cos\sigma\sin\rho$, $M_y = M\sin\sigma\sin\rho$, and $M_z = M\cos\rho$ [see Fig. 6(a) for the definition of σ and ρ], where the time-dependent angles $\sigma(t)$ and $\rho(t)$ are determined by the LL equation. Recalling that (i) $\mathbf{A}$ is an in-plane field (i.e., $A_z = 0$) and (ii) the demagnetizing field acts only on M_z and therefore only its in-plane components $H_{\text{dem},x} = M_x$ and $H_{\text{dem},y} = M_y$ exert a

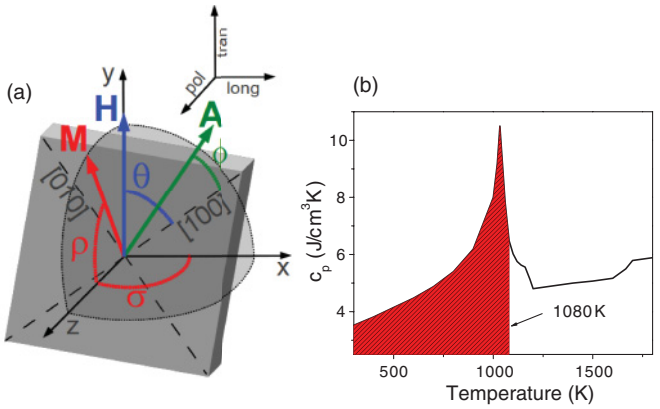

FIG. 6. (Color online) (a) Relations between magnetization **M** and fields **H** and **A** on the Fe(001) film. The external field **H** is applied along the transverse direction (y axis) at an angle θ with the [100] easy axis. The in-plane field **A** [see Eqs. (B2) and (B3)] is the combined effect of the external field and the biaxial anisotropy. It forms an angle ϕ with the [100] direction. The orientation of the magnetization vector, described in terms of spherical coordinates, is identified by the azimuth angle σ and the inclination angle ρ (with respect to the polar axis). (b) Specific heat of iron as a function of the temperature (from Ref. 36). The colored area is the numerical integral between 300 and 1080 K, resulting in an energy per unit volume of about 4200 J/cm^3.

torque, the term $\mathbf{M} \times \mathbf{H}_{\text{eff}}$ of Eq. (B1) can be simplified as follows:

$$\mathbf{M} \times \mathbf{H}_{\text{eff}} = \begin{cases} -M_z(A_y + M_y) \\ M_z(A_x + M_x) \\ M_x A_y - M_y A_x \end{cases} . \tag{B4}$$

The three Cartesian components M_x, M_y, and M_z of the magnetization are obtained by numerically solving the corresponding three coupled LL equations. However, since there are only two unknown variables [$\sigma(t)$ and $\rho(t)$], two equations are sufficient to fully determine $\mathbf{M}(t)$. It should be mentioned that, in order to achieve good agreement between the experimental data and the simulations reported in Fig. 3, a slight field-dependent damping coefficient has been assumed: in particular, we used $\alpha = 0.02$ for $H = 130$ Oe and $\alpha = 0.013$ for $H = 230$ Oe.

We conclude with a remark on the maximum local temperature induced by the optical pumping. According to our analysis based on the time-dependent modulus of magnetization (see Fig. 4), we estimated that a single laser excitation can increase the temperature of the irradiated spot up to 1000 K. To strengthen this conclusion, we can provide an argument based on simple thermal considerations. The energy E absorbed in the irradiated volume V of the Fe film can be computed as follows:

$$E/V = (\Phi/d)(1 - R)[1 - \exp(-t/\lambda)] \simeq 4200 \text{ J/cm}^3,$$

where Φ is the laser fluence of the pump (12 mJ/cm^2), d is the film thickness (8 nm), R is the film reflectivity ($\sim$0.25, experimentally measured), and λ is the optical absorption length [17 nm at a wavelength of 800 nm (Ref. 35)]. Assuming local thermal equilibrium, the energy stored in the irradiated volume can also be computed as

$$E/V = \int_{300K}^{T_{\max}} c_p dT,$$

with c_p being the specific heat of Fe and $T_{\max}$ being the maximum local temperature. Figure 6(b) reports c_p as a function of the temperature.[36] In order to achieve an energy per unit volume $E/V \simeq 4200$ J/cm^3 we have numerically integrated the curve of the specific heat between 300 K and $T_{\max} = 1080$ K. The agreement with the maximum temperature previously estimated is satisfactory.

*ettore.carpene@fisi.polimi.it

[1] C. Bunce, J. Wu, G. Ju, B. Lu, D. Hinzke, N. Kazantseva, U. Nowak, and R. W. Chantrell, Phys. Rev. B **81**, 174428 (2010).

[2] I. Radu, K. Vahaplar, C. Stamm, T. Kachel, N. Pontius, H. A. Dürr, T. A. Ostler, J. Barker, R. F. L. Evans, R. W. Chantrell, A. Tsukamoto, A. Itoh, A. Kirilyuk, Th. Rasing, and A. V. Kimel, Nature (London) **472**, 205 (2011).

[3] A. V. Kimel, A. Kirilyuk, A. Tsvetkov, R. V. Pisarev, and Th. Rasing, Nature (London) **429**, 850 (2004).

[4] A. V. Kimel, B. A. Ivanov, R. V. Pisarev, P. A. Usachev, A. Kirilyuk, and Th. Rasing, Nat. Phys. **5**, 727 (2009).

[5] Y. Acremann, C. H. Back, M. Buess, O. Portmann, A. Vaterlaus, D. Pescia, and H. Melchior, Science **290**, 492 (2000).

[6] Th. Gerrits, H. A. M. van den Berg, J. Hohlfeld, L. Bärâ, and Th. Rasing, Nature (London) **418**, 509 (2002).

[7] I. Tudosa, C. Stamm, A. B. Kashuba, F. King, H. C. Siegmann, J. Stöhr1, G. Ju, B. Lu, and D. Weller, Nature (London) **428**, 831 (2004).

[8] C. D. Stanciu, F. Hansteen, A. V. Kimel, A. Kirilyuk, A. Tsukamoto, A. Itoh, and Th. Rasing, Phys. Rev. Lett. **99**, 047601 (2007).

[9] K. Vahaplar, A. M. Kalashnikova, A. V. Kimel, D. Hinzke, U. Nowak, R. Chantrell, A. Tsukamoto, A. Itoh, A. Kirilyuk, and Th. Rasing, Phys. Rev. Lett. **103**, 117201 (2009).

[10] G. V. Astakhov, A. V. Kimel, G. M. Schott, A. A. Tsvetkov, A. Kirilyuk, D. R. Yakovlev, G. Karczewski, W. Ossau, G. Schmidt, L. W. Molenkamp, and Th. Rasing, Appl. Phys. Lett. **86**, 152506 (2005).

[11] Y. Zhu, X. Zhang, T. Li, X. Huang, L. Han, and J. Zhao, Appl. Phys. Lett. **95**, 052108 (2009).

[12] A. H. M. Reid, G. V. Astakhov, A. V. Kimel, G. M. Schott, W. Ossau, K. Brunner, A. Kirilyuk, L. W. Molenkamp, and Th. Rasing, Appl. Phys. Lett. **97**, 232503 (2010).

[13] G. Bertotti, *Hysteresis in Magnetism* (Academic, San Diego, 1998).

[14] R. P. Cowburn, S. J. Gray, J. Ferré, J. A. C. Bland, and J. Miltat, J. Appl. Phys. **78**, 7210 (1995).

[15]The choice of $\theta \simeq 44^\circ$ is experimentally justified. Details can be found in Appendix A.
[16]E. Beaurepaire, J.-C. Merle, A. Daunois, and J.-Y. Bigot, Phys. Rev. Lett. **76**, 4250 (1996).
[17]M. van Kampen, C. Jozsa, J. T. Kohlhepp, P. LeClair, L. Lagae, W. J. M. de Jonge, and B. Koopmans, Phys. Rev. Lett. **88**, 227201 (2002).
[18]J.-Y. Bigot, M. Vomir, L. H. F. Andrade, and E. Beaurepaire, Chem. Phys. **318**, 137 (2005).
[19]B. Koopmans, J. J. M. Ruigrok, F. DallaLonga, and W. J. M. de Jonge, Phys. Rev. Lett. **95**, 267207 (2005).
[20]J.-Y. Bigot, M. Vomir, and E. Beaurepaire, Nat. Phys. **5**, 515 (2009).
[21]G. P. Zhang, W. Hübner, G. Lefkidis, Y. Bai, and T. F. George, Nat. Phys. **5**, 499 (2009).
[22]E. Carpene, E. Mancini, C. Dallera, M. Brenna, E. Puppin, and S. De Silvestri, Phys. Rev. B **78**, 174422 (2008).
[23]M. Vomir, L. H. F. Andrade, L. Guidoni, E. Beaurepaire, and J.-Y. Bigot, Phys. Rev. Lett. **94**, 237601 (2005).
[24]H. F. Ding, S. Pütter, H. P. Oepen, and J. Kirschner, J. Magn. Magn. Mater. **212**, L5 (2000).
[25]P. Vavassori, Appl. Phys. Lett. **77**, 1605 (2000).
[26]E. Carpene, E. Mancini, D. Dazzi, C. Dallera, E. Puppin, and S. De Silvestri, Phys. Rev. B **81**, 060415(R) (2010).
[27]E. Carpene, E. Mancini, C. Dallera, E. Puppin, and S. De Silvestri, J. Appl. Phys. **108**, 063919 (2010).
[28]L. Landau and E. Lifshitz, Phys. Z. Union **8**, 153 (1935).
[29]H.-P. Klein and E. Kneller, Phys. Rev. **144**, 372 (1966).
[30]S. D. Hanham, A. S. Arrott, and B. Heinrich, J. Appl. Phys. **52**, 1941 (1981).
[31]B. Heinrich and J. F. Cochran, Adv. Phys. **42**, 523 (1993).
[32]A. J. Melmed and J. J. Carroll, J. Vac. Sci. Technol. **10**, 164 (1973).
[33]M. Rubinstein, F. J. Rachford, W. W. Fuller, and G. A. Prinz, Phys. Rev. B **37**, 8689 (1988).
[34]Z. J. Yang and M. R. Scheinfein, J. Appl. Phys. **74**, 6810 (1993).
[35]*Handbook of Chemistry and Physics*, edited by R. C. Weast and M. J. Astle (CRC Press, Boca Raton, 1983).
[36]*Thermophisical Properties of Matter*, edited by Y. S. Touloukian and C. Y. Ho (Plenum, New York, 1970), Vols. 1 and 4.